Version of Record: https://www.sciencedirect.com/science/article/pii/S2452213922002947
Manuscript_b17aac880b829ea692a069c81a2a733b

Additive manufacturing of magnetocaloric (La,Ce)(Fe,Mn,Si)$_{13}$-H particles via polymer-based composite filaments

Á. Díaz-García[1], J. Revuelta[1], L.M. Moreno-Ramírez[1], J.Y. Law[1], C. Mayer[2], V. Franco[1,*]

[1]Departamento de Física de la Materia Condensada, ICMS-CSIC, Universidad de Sevilla, P.O. Box 1065. 41080, Sevilla, Spain.

[2] Aubert & Duval, Usine des Ancizes, Rue des villas, BP1, Les Ancizes 63770, France

* Corresponding author. Email: vfranco@us.es

Abstract
Additive manufacturing could be an excellent way of shaping magnetocaloric heat exchangers in magnetic refrigerators. However, the metal additive manufacturing techniques present the serious limitation that the melting of a magnetocaloric material can cause its transformation and the loss of functionality. Fused deposition modeling using polymer-based composite filaments is presented as a promising alternative as temperatures are low enough to preserve the magnetocaloric material. To prove this claim, a polymer-based composite filament containing 55 wt.% of (La,Ce)(Fe,Mn,Si)$_{13}$-H magnetocaloric fillers has been manufactured using custom-made polymer capsules as the feedstock for the extrusion. Both adiabatic temperature change and isothermal entropy change have been characterized for the fillers, as-prepared filaments and as-printed parts, indicating that the magnetocaloric material functionality is not altered along the whole process. Printing resolution is comparable to the raw PLA filament.

Keywords
Additive manufacturing, Fused deposition modeling, Magnetocaloric composite

1 Introduction

Magnetocaloric effect (MCE) is a functionality that can be used for energy efficient refrigeration [1]. High-performance MCE materials, usually intermetallics with first-order phase transition (FOPT), inevitably exhibit poor processability, which limits their incorporation in actual devices. Their brittleness and the volume changes due to the FOPT makes it challenging to develop durable heat transfer parts of optimal shapes using traditional manufacturing methods [2][3]. Additive manufacturing (AM), whose rapid advances are position this technology in a relevant place for the manufacturing of final functional parts [4][5], could be instrumental in overcoming these issues of magnetocaloric regenerators [6][7]. Although there have been works that directly print from raw metallic powders, e.g., laser or electron beam melting, the additional melting of the magnetocaloric material could lead to compositional changes or lose the desired phase that mainly contribute to the large MCE. These would lead to alteration in the overall material performance, which is highly undesirable. This has shown to be relevant for Heusler alloys [8][9][10][11], (Mn,Fe)$_2$(P,Si) [12][13] or La(Fe,Si)$_{13}$ [6][7][14][15]. Very recently, injection molding and extrusion-based AM are starting to be used for printing magnetocaloric regenerators with the hypothesis that the lower processing temperatures prevent the highly desirable phases that contribute to high MCE performance from being altered [16][17][18]. However, a full characterization of the magnetocaloric performance and how it evolves along the whole fabrication route is still missing.

Focusing on La(Fe,Si)$_{13}$ materials, which present excellent magnetocaloric responses together with reduced hysteresis, different attempts have been performed on extrusion-based AM. S. Wieland et al. [19] successfully mixed high loads of La(Fe,Si)$_{13}$ powder with a mixture of polyethylene binder and waxes for extrusion molding. Chemical and thermal debinding have been performed prior to thermal annealing and hydrogenation processes on the final

manufactured parts to improve the $NaZn_{13}$-type structure (1:13) content and to obtain the MCE response close to room temperature (RT). The annealing also served as the sintering of the molded parts, but it causes several distortions of some pieces as well as difficulties in optimizing the material and in preventing the appearance of oxides. J. Lanzarini et al. [20] mixed $(La,Ce)(Fe,Mn,Si)_{13}$-H powders with thermoplastic polypropylene for injection molding without further debinding or sintering processes. It was found that the transition temperature of the powder is affected by the mixing temperature with the dehydrogenation occurring from 473 K.

Fused deposition modeling (FDM) is also an extrusion-based AM popular procedure that uses thermoplastic filaments that can contain fillers for the 3D printing of functional parts [21]. Extrusion temperatures of typical thermoplastics do not go beyond 573 K (300 ºC), being low enough to preserve the properties of most of the FOPT magnetocaloric materials. The most common thermoplastic for FDM is polylactic acid (PLA) with extrusion and printing temperatures of ~ 473 K. We have recently shown that composite filaments fabricated using PLA capsules filled with maraging steel particles as the feedstock for extrusion show very good uniformity, both dimensionally and of particle concentration. At the same time, this procedure helps us reduce the required extrusion temperatures with respect to pure PLA [22][23], which could be a key for not reaching dehydrogenation temperatures of magnetocaloric powders.

In this work, PLA-based composite filament containing 55 wt.% of $(La,Ce)(Fe,Mn,Si)_{13}$-H fillers has been manufactured through the novel encapsulation method presented in [22]. The composite filament allows high resolution printings using a commercial desktop 3D printer. It is shown that the isothermal entropy changes of the as-extruded and printed composites are proportional to the amount of fillers contained, indicating that the fraction of 1:13 phase and hydrogenation of the powder are intact after the whole fabrication process. Direct measurements of the adiabatic temperature change show the influence of the polymer in reducing the total temperature change of the composite due to the heat capacity of the polymer being different (and larger) from that of the fillers.

2 Materials and methods

The initial raw materials for the extrusion are standard grade PLA pellets and heat treated and hydrogenated gas-atomized $(La,Ce)(Fe,Mn,Si)_{13}$-H powder with composition $La_{0.7}Ce_{0.3}(Fe_{0.885}Mn_{0.015}Si_{0.1})_{13}H$ provided by Aubert & Duval (France). The microstructural characterization of the raw powder has been performed by scanning electron microscopy (SEM) using a FEI Teneo microscope and by X-ray diffraction (XRD) using a D8 ADVANCE A25 diffractometer with Cu-Kα radiation. **Figure 1 (a)-(b)** show the SEM and XRD results of the $(La,Ce)(Fe,Mn,Si)_{13}$-H powder. The powder exhibits a wide range of particle sizes with predominantly irregular shapes due to the decrepitation that the hydrogenation caused [24,25]. Further Rietveld refinement of the XRD pattern (**Figure 1 (b)**) shows a 5.4(6) wt. % of α-Fe impurities in addition to the desired 1:13 phase. The α-Fe phase, with a Curie transition around 1050 K, will not contribute to the MCE in the vicinity of RT.

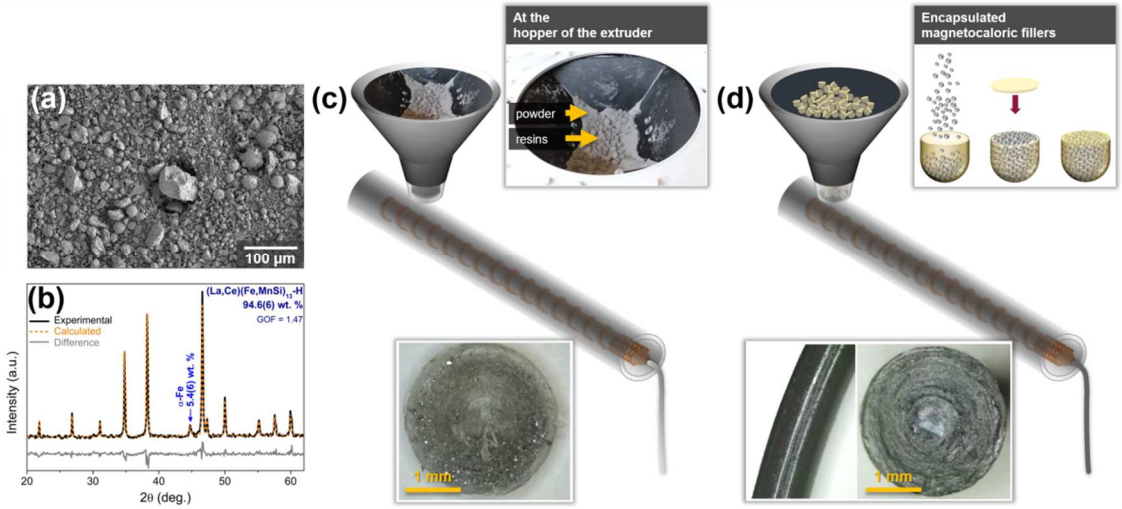

Figure 1. (a) SEM micrograph and (b) XRD including its Rietveld refinement data of the raw (La,Ce)(Fe,Mn,Si)$_{13}$-H powder. (c) Schematic presentations and accompanying photos of the feedstock and resulted composite filaments fabricated from conventional and (d) customized feedstock methodologies. Images at the bottom of (c) and (d) corresponds to the cross-section of the composite filaments manufactured by each of these methods.

A novel methodology of fabricating high quality magnetic composite filaments with good compositional control have been followed [22]. In contrast to the conventional way which uses feedstock that mixes polymers with fillers as schematically presented in **Figure 1 (c)** and leads to non-homogeneous composite filaments**,** our approach uses custom-made polymer capsules filled with functional powder as the feedstock for the filament extrusion as shown in **Figure 1 (d)**. Following this method, PLA capsules were printed using a Ultimaker S5 printer. They were filled with the (La,Ce)(Fe,Mn,Si)$_{13}$-H powder with a nominal composition of 60 wt. %. The composite filament of diameter of 1.75 mm was extruded using a single-screw extruder (3devo NEXT 1.0 ADVANCED). It was necessary to lowering the temperatures of the 4 extruder heaters by ~15 K with respect to those predefined for PLA. Otherwise, the composite filament exits the nozzle in a highly fluid state that prevents spooling. This phenomenon is associated with the lack of particle agglomerations and the "ball-bearing effect" [23]. With this methodology, smooth and uniform magnetocaloric composite filament was obtained as observed from the photos provided in **Figure 1 (d).** A Prusa i3 MK3S 3D printer was used for testing the printability of the fabricated PLA+ (La,Ce)(Fe,Mn,Si)$_{13}$-H composite filament. The thermal behavior of the composite filament was characterized by thermogravimetry analysis (TGA) using a TA Instruments Q600 thermobalance and by differential scanning calorimetry (DSC) using a TA Instruments Q20 calorimeter.

The isothermal entropy change, ΔS_{iso}, was indirectly determined from isothermal magnetization measurements using the Maxwell relation [1]. Measurements were performed with a LakeShore 7407 vibrating sample magnetometer (VSM) using a discontinuous measurement protocol [26–29]. The temperature change of the samples was measured using a home-made device based on infrared thermography. The base temperature was modified by passing a cooling fluid through a sample holder onto which the sample is attached using a large thermal conductivity varnish. A sinusoidal oscillating magnetic field between 0 and 0.75 T at 0.5 Hz was applied with an electromagnet. The temperature changes of the sample were recorded using an infrared camera. A lock-in technique [30] consisting in the detection of the temperature response of the sample at the same frequency of the oscillating field is performed by numerical processing the experimental data by multiplying it to the sinusoidal field and extracting the DC component of the resulting signal. In this way, from a noise-equivalent temperature (NETD) of 140 mK

indicted by the manufacturer, the noise level in the lock-in processed response is reduced to 7 mK. As the field was continuously oscillated, only the reversible response of the sample, ΔT_{rev}, was detected via lock-in thermography.

3 Results and discussions

3.1 Thermal behavior of the filament

The TGA curves of the raw PLA and composite (**Figure 2 (a)**) present the latter with 55 wt. % of (La,Ce)(Fe,Mn,Si)$_{13}$-H upon the thermal decomposition of the PLA. The thermal degradation of PLA significantly shifts to lower temperatures (around -100 K) with the addition of these fillers. This has been observed for other PLA-based composites incorporating metallic fillers in the literature [23][31], which is likely due to the capability of some metallic fillers for reducing the activation energy related to the thermal degradation of the polymer [31].

Figure 2 (b) shows the DSC curves upon heating and cooling of the raw powder and composite in the temperature region of the thermomagnetic transition of (La,Ce)(Fe,Mn,Si)$_{13}$-H. The large endothermic peak observed for the raw powder indicates the occurrence of the FOPT at RT. This is also observed in the DSC curves of the composite although the peak is significantly reduced. One reason for this difference is that the total mass of the composite sample, including the mass of polymer, is accounted in the DSC curve. However, the latent heat due to the thermomagnetic phase transition of the raw powder cannot be recovered simply by normalizing the curve of the composite to the mass of (La,Ce)(Fe,Mn,Si)$_{13}$-H contained. The polymer, on having a higher heat capacity than that of the fillers, results in the need for more heat per unit mass in the composite with respect to that of the raw powder to attain the same temperature change.

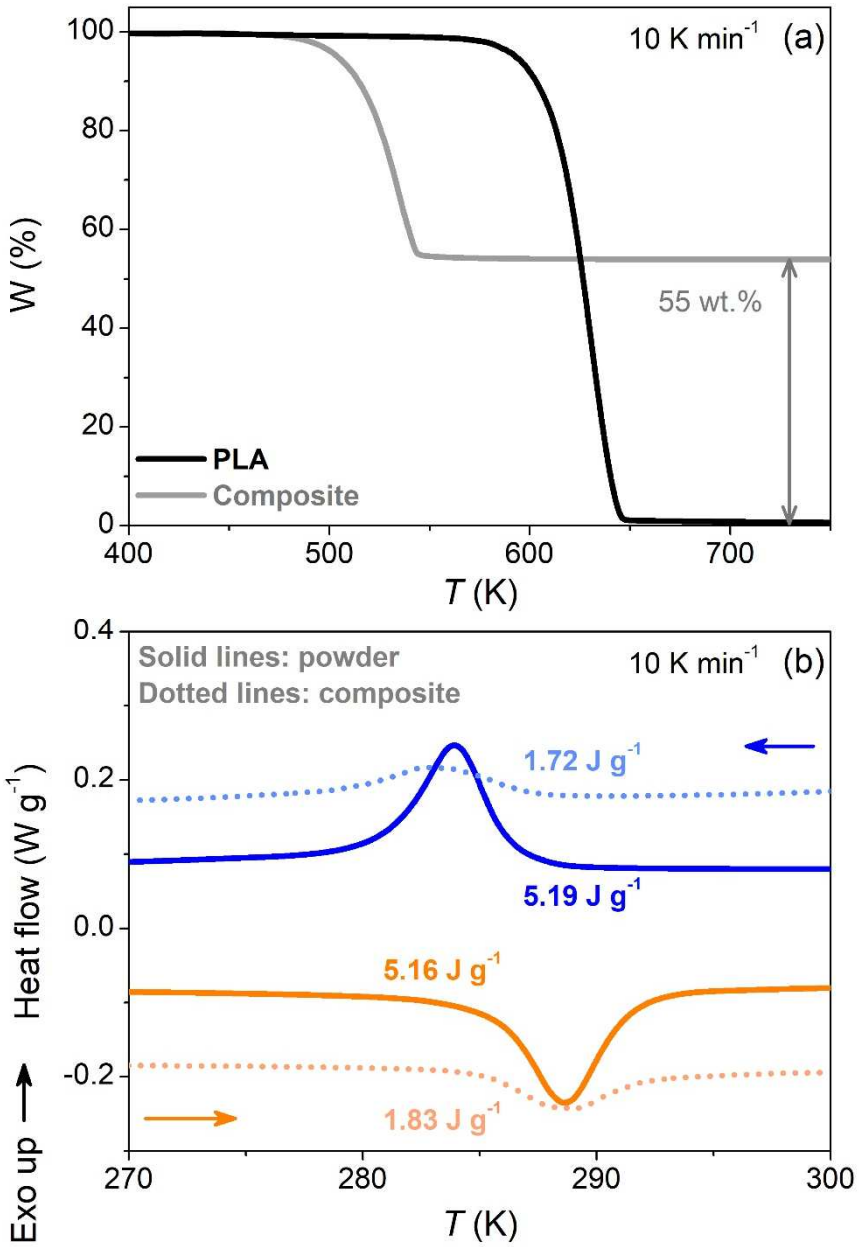

Figure 2. **(a)** TGA and **(b)** DSC curves of raw (La,Ce)(Fe,Mn,Si)$_{13}$-H powder and PLA + (La,Ce)(Fe,Mn,Si)$_{13}$-H composite.

3.2 3D printing

Figure 3 (a) and **(b)** show the same "snowflake" design printed using a commercial PLA filament and the manufactured PLA+ (La,Ce)(Fe,Mn,Si)$_{13}$-H filament, respectively. The printing with PLA was done using the corresponding predefined 483 K (210 ºC), while in the case of the (La,Ce)(Fe,Mn,Si)$_{13}$-H filament the printing temperature had to be lowered down to 455 K (182 ºC). Otherwise, the (La,Ce)(Fe,Mn,Si)$_{13}$-H filament exits the nozzle of the printer with very high fluidity leading to poor resolution in the different printed layers when using the printing temperature of PLA. The lowering of the manufacturing and printing temperatures is positive as they are below the dehydrogenation threshold and also would require less energy, which would be very relevant if the process is scaled to industry. It is expected that the lowered extrusion temperatures would also have less effect on the properties of the functional fillers.

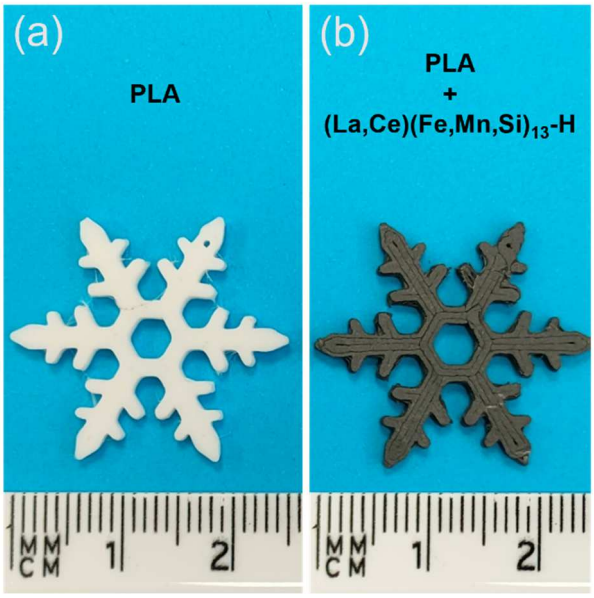

Figure 3. Printed objects using **(a)** PLA and **(b)** the PLA+(La,Ce)(Fe,Mn,Si)$_{13}$-H composite filaments.

3.3 Indirect magnetocaloric response

The $\Delta S_{iso}(T)$ curves upon heating and cooling of the (La,Ce)(Fe,Mn,Si)$_{13}$-H powder, as-extruded composite and 3D-printed part are presented in **Figure 4 (a)**. The heating and cooling $\Delta S_{iso}(T)$ curves overlap one another for the as-extruded composite and 3D-printed samples. Upon normalizing the results of composite samples with 55 wt. % of (La,Ce)(Fe,Mn,Si)$_{13}$-H to consider only the active MCE material (according to TGA results), their $\Delta S_{iso}(T)$ curves overlap with those of the powder as observed in the inset of **Figure 4 (a)**. The temperature corresponding to the heating and cooling peaks are found at 289 K (also the same for the composite samples), indicating a negligible thermal hysteresis for a field of 1.5 T. Therefore, the filament manufacturing preserves both the amount of 1:13 phase and the hydrogenation of (La,Ce)(Fe,Mn,Si)$_{13}$-H fillers. Retaining the hydrogenation intact is especially challenging since it could be lost due to the heating, which would lead to lowering the transition temperature of La(Fe,Si)$_{13}$ system to ~ 200 K.

The FOPT of the used (La,Ce)(Fe,Mn,Si)$_{13}$-H powder has been identified by the criterion of the overshoot of exponent n above 2 [32], as presented in **Figure 4 (b)**. The overshoot feature is clearly observed also for the composite samples, further confirming the retainment of the properties of the powder after the whole manufacturing process. At the ferromagnetic region in the low temperature range, the n values of the composite samples are slightly above the theoretical n =1 due to the higher demagnetizing factor in comparison to the compacted powder [33][34]. In the paramagnetic region after the phase transition, the exponent n is below the theoretical value of n =2 for all the samples due to the influence of ferromagnetic α-Fe impurities as found in the XRD analysis of **Figure 1 (a)**.

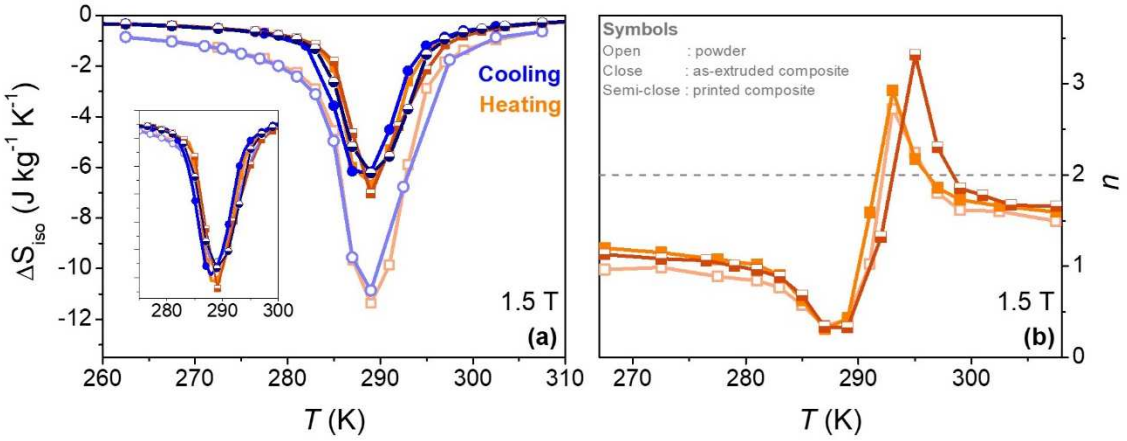

Figure 4. **(a)** $\Delta S_{iso}(T)$ and **(b)** $n(T)$ for 1.5 T of (La,Ce)(Fe,Mn,Si)$_{13}$-H powder (open symbols), as-extruded composite (close symbols) and 3D-printed part (semi-close symbols). **Inset** in (a) shows the effect of normalization with 55 wt. % filler on the $\Delta S_{iso}(T)$ results of the composite samples**.**

3.4 Direct magnetocaloric response

The ΔT_{rev} of a compact of the raw powders and a printed part using the composite filament are presented in **Figure 5**. In agreement with the results of ΔS_{iso}, the MCE of the powders remains after extrusion, with curves that have qualitatively the same shape. However, in contrast with the $\Delta S_{iso}(T)$ results, both curves do not become identical if they are normalized by the mass of (La,Ce)(Fe,Mn,Si)$_{13}$-H: the ratio $\Delta T_{rev,composite}/\Delta T_{rev,powder} = 0.45$, while the mass fraction of powders is 0.55. This is because the total heat supplied by the MCE, $T\,\Delta S_{iso}$, is used in changing the temperature of both phases in the case of the composite and the polymer has higher heat capacity than the fillers. This agrees with the DSC results shown in **Figure 2 (b)**, where a decrease of the transformation peak and a rounding of it are observed. Therefore, the way to obtain larger ΔT_{rev} would be to decrease the heat capacity of the polymer (which implies controlling the composition of this phase) and to decrease the fraction of polymer (which is limited by the printability of the filament).

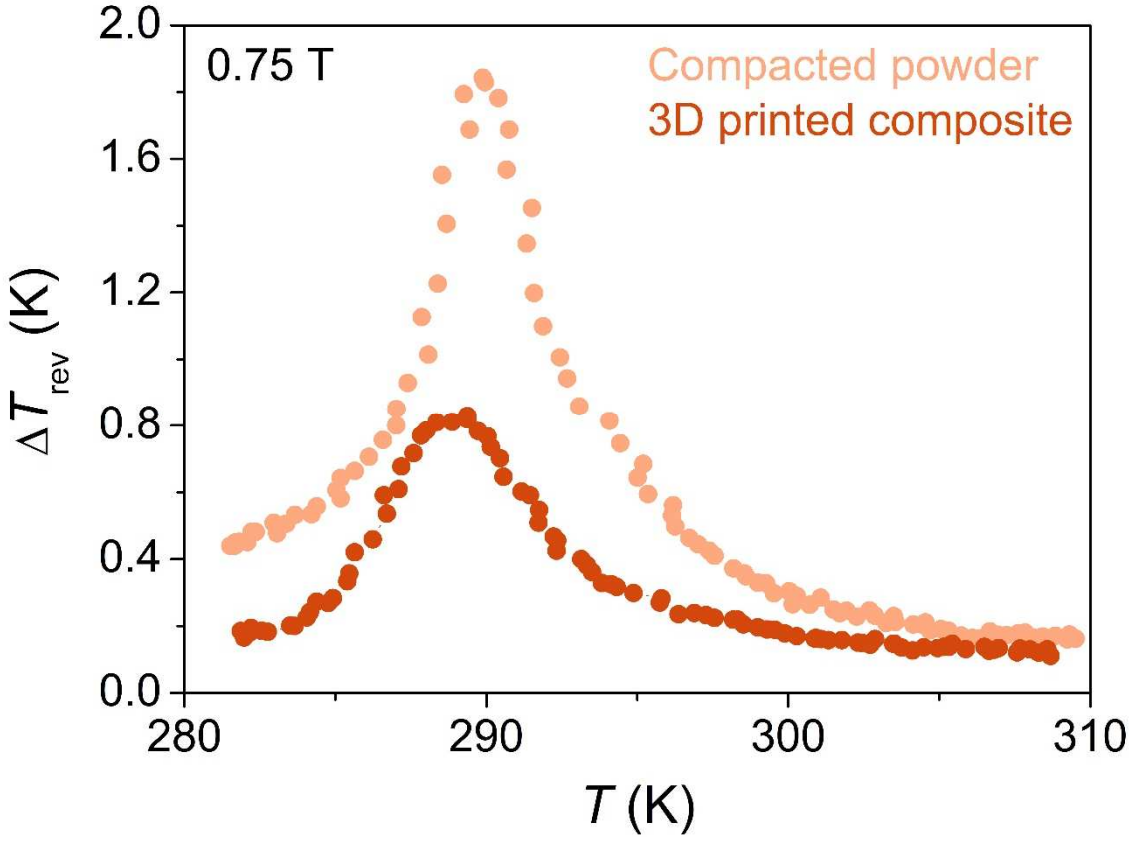

Figure 5. IR-thermography figures of compacted (La,Ce)(Fe,Mn,Si)$_{13}$-H powder and 3D printed PLA+ (La,Ce)(Fe,Mn,Si)13-H samples.

4 Conclusions

A PLA-based magnetocaloric composite filament with 55 wt.% of (La,Ce)(Fe,Mn,Si)$_{13}$-H has been manufactured using PLA capsules filled with (La,Ce)(Fe,Mn,Si)$_{13}$-H particles as the feedstock for the extrusion. A 3D printed piece with similar printing resolution to that of pure PLA is achieved with the composite filament once the printing conditions are optimized. The composites show a ΔS_{iso} proportional to the mass of fillers, showing that the fraction of the 1:13 phase and hydrogenation remain unaltered after all the fabrication processes. For this, the reduction of extrusion temperature below the dehydrogenation temperature, achieved with our original manufacturing process, is key. Lock-in infrared thermography shows a ΔT_{rev} of 0.8 K in a printed sample for 0.75 T. This response is 45% of that of the raw powder, highlighting the contribution of the heat capacity of the polymer. We have shown that functional magnetocaloric parts can be printed by FDM using composite filaments manufactured with our encapsulation method, with potential improvement of functionality by controlling the heat capacity of the polymer matrix.

Acknowledgements

Work supported by Grant PID2019-105720RB-I00 funded by MCIN/AEI /10.13039/501100011033, Consejería de Economía, Conocimiento, Empresas y Universidad de la Junta de Andalucía (grant P18-RT-746), and Air Force Office of Scientific Research (FA8655-21-1-7044).

References

[1] V. Franco, J.S. Blázquez, J.J. Ipus, J.Y. Law, L.M. Moreno-Ramírez, A. Conde, Magnetocaloric effect: From materials research to refrigeration devices, Prog. Mater. Sci. 93 (2018) 112–232. https://doi.org/10.1016/j.pmatsci.2017.10.005.

[2] M.S. Kamran, J. Sun, Y.B. Tang, Y.G. Chen, J.H. Wu, H.S. Wang, Numerical investigation of room temperature magnetic refrigerator using microchannel regenerators, Appl. Therm. Eng. 102 (2016) 1126–1140. https://doi.org/10.1016/j.applthermaleng.2016.02.085.

[3] T. Lei, K. Engelbrecht, K.K. Nielsen, C.T. Veje, Study of geometries of active magnetic regenerators for room temperature magnetocaloric refrigeration, Appl. Therm. Eng. 111 (2017) 1232–1243. https://doi.org/10.1016/j.applthermaleng.2015.11.113.

[4] C. Zhang, F. Chen, Z. Huang, M. Jia, G. Chen, Y. Ye, Y. Lin, W. Liu, B. Chen, Q. Shen, L. Zhang, E.J. Lavernia, Additive manufacturing of functionally graded materials: A review, Mater. Sci. Eng. A. 764 (2019) 138209. https://doi.org/10.1016/j.msea.2019.138209.

[5] A.P. Fagundes, J.O. de B. Lira, N. Padoin, C. Soares, H.G. Riella, Additive manufacturing of functional devices for environmental applications: A review, J. Environ. Chem. Eng. 10 (2022) 108049. https://doi.org/10.1016/j.jece.2022.108049.

[6] K. Navickaitė, J. Liang, C. Bahl, S. Wieland, T. Buchenau, K. Engelbrecht, Experimental characterization of active magnetic regenerators constructed using laser beam melting technique, Appl. Therm. Eng. 174 (2020) 115297. https://doi.org/10.1016/j.applthermaleng.2020.115297.

[7] A.E.-M.A. Mohamed, M. Jeong, R.S. Sheridan, M.M. Attallah, Enabling high efficiency magnetic refrigeration using laser powder bed fusion of porous LaCe(Fe,Mn,Si)13 structures, Addit. Manuf. 51 (2022) 102620. https://doi.org/10.1016/j.addma.2022.102620.

[8] J. Toman, P. Müllner, M. Chmielus, Properties of as-deposited and heat-treated Ni-Mn-Ga magnetic shape memory alloy processed by directed energy deposition, J. Alloys Compd. 752 (2018) 455–463. https://doi.org/10.1016/j.jallcom.2018.04.059.

[9] V. Laitinen, A. Sozinov, A. Saren, A. Salminen, K. Ullakko, Laser powder bed fusion of Ni-Mn-Ga magnetic shape memory alloy, Addit. Manuf. 30 (2019) 100891. https://doi.org/10.1016/j.addma.2019.100891.

[10] F. Nilsén, I.F. Ituarte, M. Salmi, J. Partanen, S.-P. Hannula, Effect of process parameters on non-modulated Ni-Mn-Ga alloy manufactured using powder bed fusion, Addit. Manuf. 28 (2019) 464–474. https://doi.org/10.1016/j.addma.2019.05.029.

[11] F. Scheibel, C. Lauhoff, S. Riegg, P. Krooß, E. Bruder, E. Adabifiroozjaei, L. Molina-Luna, S. Böhm, Y.I. Chumlyakov, T. Niendorf, O. Gutfleisch, On the Impact of Additive Manufacturing Processes on the Microstructure and Magnetic Properties of Co–Ni–Ga Shape Memory Heusler Alloys, Adv. Eng. Mater. 2200069 (2022) 2200069. https://doi.org/10.1002/adem.202200069.

[12] T. Christiaanse, E. Brück, Proof-of-Concept Static Thermomagnetic Generator Experimental Device, Metall. Mater. Trans. E. 1 (2014) 36–40. https://doi.org/10.1007/s40553-014-0006-9.

[13] X. Miao, W. Wang, H. Liang, F. Qian, M. Cong, Y. Zhang, A. Muhammad, Z. Tian, F. Xu, Printing (Mn,Fe)2(P,Si) magnetocaloric alloys for magnetic refrigeration applications, J. Mater. Sci. 55 (2020) 6660–6668. https://doi.org/10.1007/s10853-020-04488-8.

[14] J.D. Moore, D. Klemm, D. Lindackers, S. Grasemann, R. Träger, J. Eckert, L. Löber, S. Scudino, M. Katter, A. Barcza, K.P. Skokov, O. Gutfleisch, Selective laser melting of La(Fe,Co,Si) 13 geometries for magnetic refrigeration, J. Appl. Phys. 114 (2013) 043907. https://doi.org/10.1063/1.4816465.

[15] K.J. Merazzo, A.C. Lima, M. Rincón-Iglesias, L.C. Fernandes, N. Pereira, S. Lanceros-Mendez, P. Martins, Magnetic materials: a journey from finding north to an exciting printed future, Mater. Horizons. 8 (2021) 2654–2684. https://doi.org/10.1039/D1MH00641J.

[16] K.N. Al-Milaji, S. Gupta, V.K. Pecharsky, R. Barua, H. Zhao, R.L. Hadimani, Differential effect of magnetic alignment on additive manufacturing of magnetocaloric particles, AIP Adv. 10 (2020) 015052. https://doi.org/10.1063/1.5130028.

[17] B. Rodríguez-Crespo, D. Salazar, S. Lanceros-Méndez, V. Chernenko, Development and magnetocaloric properties of Ni(Co)-Mn-Sn printing ink, J. Alloys Compd. 917 (2022) 165521. https://doi.org/10.1016/j.jallcom.2022.165521.

[18] V. Sharma, L. Balderson, R. Heo, O. Bishop, C.S.M. Hunt, E.E. Carpenter, R.L. Hadimani, H. Zhao, R. Barua, Room-temperature polymer-assisted additive manufacturing of microchanneled magnetocaloric structures, J. Alloys Compd. 920 (2022) 165891. https://doi.org/10.1016/j.jallcom.2022.165891.

[19] S. Wieland, F. Petzoldt, Powder-extrusion and sintering of magnetocaloric LaCe(FeMnSi) 13 alloy, J. Alloys Compd. 719 (2017) 182–188. https://doi.org/10.1016/j.jallcom.2017.05.168.

[20] J. Lanzarini, T. Barriere, M. Sahli, J.C. Gelin, A. Dubrez, C. Mayer, M. Pierronnet, P. Vikner, Thermoplastic filled with magnetocaloric powder, Mater. Des. 87 (2015) 1022–1029. https://doi.org/10.1016/j.matdes.2015.08.057.

[21] P.M. Angelopoulos, M. Samouhos, M. Taxiarchou, Functional fillers in composite filaments for fused filament fabrication: A review, Mater. Today Proc. 37 (2019) 4031–4043. https://doi.org/10.1016/j.matpr.2020.07.069.

[22] Á. Díaz-García, J.Y. Law, A. Cota, A. Bellido-Correa, J. Ramírez-Rico, R. Schäfer, V. Franco, Novel procedure for laboratory scale production of composite functional filaments for additive manufacturing, Mater. Today Commun. 24 (2020) 101049. https://doi.org/10.1016/j.mtcomm.2020.101049.

[23] Á. Díaz-García, J.Y. Law, M. Felix, A. Guerrero, V. Franco, Functional, thermal and rheological properties of polymer-based magnetic composite filaments for additive manufacturing, Mater. Des. 219 (2022) 110806. https://doi.org/10.1016/j.matdes.2022.110806.

[24] J. Liu, J.D. Moore, K.P. Skokov, M. Krautz, K. Löwe, A. Barcza, M. Katter, O. Gutfleisch, Exploring La(Fe,Si)13-based magnetic refrigerants towards application, Scr. Mater. 67 (2012) 584–589. https://doi.org/10.1016/j.scriptamat.2012.05.039.

[25] M. Krautz, K. Skokov, T. Gottschall, C.S. Teixeira, A. Waske, J. Liu, L. Schultz, O. Gutfleisch, Systematic investigation of Mn substituted La(Fe,Si)13 alloys and their hydrides for room-temperature magnetocaloric application, J. Alloys Compd. 598 (2014) 27–32. https://doi.org/10.1016/j.jallcom.2014.02.015.

[26] L. Tocado, E. Palacios, R. Burriel, Entropy determinations and magnetocaloric parameters in systems with first-order transitions: Study of MnAs, J. Appl. Phys. 105 (2009) 093918. https://doi.org/10.1063/1.3093880.

[27] L. Caron, Z.Q. Ou, T.T. Nguyen, D.T. Cam Thanh, O. Tegus, E. Brück, On the determination of the magnetic entropy change in materials with first-order transitions, J.

Magn. Magn. Mater. 321 (2009) 3559–3566. https://doi.org/10.1016/j.jmmm.2009.06.086.

[28] B. Kaeswurm, V. Franco, K.P. Skokov, O. Gutfleisch, Assessment of the magnetocaloric effect in La,Pr(Fe,Si) under cycling, J. Magn. Magn. Mater. 406 (2016) 259–265. https://doi.org/10.1016/j.jmmm.2016.01.045.

[29] J.H. Chen, A. Us Saleheen, P.W. Adams, D.P. Young, N. Ali, S. Stadler, On entropy determination from magnetic and calorimetric experiments in conventional giant magnetocaloric materials, J. Appl. Phys. 123 (2018) 0–7. https://doi.org/10.1063/1.5016858.

[30] P.A. Temple, An introduction to phase-sensitive amplifiers: An inexpensive student instrument, Am. J. Phys. 43 (1975) 801–807. https://doi.org/10.1119/1.9690.

[31] J.-Y. Lee, Y. Liao, R. Nagahata, S. Horiuchi, Effect of metal nanoparticles on thermal stabilization of polymer/metal nanocomposites prepared by a one-step dry process, Polymer (Guildf). 47 (2006) 7970–7979. https://doi.org/10.1016/j.polymer.2006.09.034.

[32] J.Y. Law, V. Franco, L.M. Moreno-Ramírez, A. Conde, D.Y. Karpenkov, I. Radulov, K.P. Skokov, O. Gutfleisch, A quantitative criterion for determining the order of magnetic phase transitions using the magnetocaloric effect, Nat. Commun. 9 (2018) 2680. https://doi.org/10.1038/s41467-018-05111-w.

[33] J.M.D. Coey, Magnetism and Magnetic Materials, Cambridge University Press, 2001. https://doi.org/10.1017/CBO9780511845000.

[34] C. Romero-Muñiz, J.J. Ipus, J.S. Blázquez, V. Franco, A. Conde, Influence of the demagnetizing factor on the magnetocaloric effect: Critical scaling and numerical simulations, Appl. Phys. Lett. 104 (2014) 252405. https://doi.org/10.1063/1.4885110.